Small-Signal Analysis of Multi-Phase Interleaved Boost Converter with Coupled Inductor

Hwi-Beom Shin*, Eun-Sung Jang*, Se-Kyo Chung*, and Hyun-Woo Lee**
* School of Electrical & Electronic Engineering, Gyeongsang National University
900 Gazwa-dong, Chinju, Gyeongnam, 660-701, KOREA
** School of Electrical Engineering & Computer Science, Kyungnam University
Masan, Gyeongnam, 7 02-701, KOREA

ABSTRACT

This paper addresses the small-signal analysis of the multi-phase interleaved boost converter with the coupled inductors operated in the continuous inductor current mode. The generalized and analytical expressions for the transfer functions of interest are derived for various inductor couplings. The dynamic characteristics are analyzed according to the inductor couplings and verified experimentally. The proposed frequency models will be very useful to design the dynamic controllers of the multi-phase interleaved boost converters.

1. INTRODUCTION

Recently, the interleaved boost converter (IBC) has been studied for the application to power factor correction circuits and interface between battery source or the photovoltaic array and the dc bus of AC inverter. The IBC is composed of several identical boost converters connected in parallel. The converters are controlled by the interleaved switching signals, which have the same switching frequency and the same phase shifting. By virtue of paralleling the converters, the input current can be shared among the cells or phases, so that high reliability and efficiency in power electronic systems can be obtained. As a consequence of the interleaving operation, the IBC exhibits both lower current ripple at the input side and lower voltage ripple at the output side [1]-[2].

In this paper, the generalized small-signal model of the multi-phase IBC with coupled inductors is developed by using Lunze's transformation, which enables to consider the inductor currents of the multi-phase as the common-mode and differential mode currents, separately. The common-mode current is useful when the phases are symmetrical. The converter is assumed to operate in the continuous inductor current mode. The generalized and explicit expressions for the transfer functions of interest are derived and characterized according to the inductor couplings. The generalized analysis for converter performance is verified through the experimental results.

2. GENERALIZED AVERAGED STATE MODEL AND SMALL SIGNAL ANALYSIS

Fig. 1 shows the multi-phase IBC with coupled inductors in which $2N$ boost converters are connected in parallel. Each converter consists of a coupled inductor, active switch, and diode. It is assumed that the parallel converters are symmetrical and operate in the continuous inductor current mode. Considering the polarity of the coupling inductors as shown in Fig. 1, the dynamics of the inductor currents can be written as

$$L_1\frac{di_{L,2k-1}}{dt}+L_m\sum_{j=1}^{N}\frac{di_{L,2j-1}}{dt}+\rho L_m\sum_{j=1}^{N}\frac{di_{L,2j}}{dt} =-ri_{L,2k-1}-s_{2k-1}'v_0=V_g$$

$$L_1\frac{di_{L,2k}}{dt}+\rho L_m\sum_{j=1}^{N}\frac{di_{L,2j-1}}{dt}+L_m\sum_{j=1}^{N}\frac{di_{L,2j}}{dt} =-ri_{L,2k}-s_{2k-1}'v_0=V_g \qquad (1)$$

where $s_k'=1-s_k, k=1,2,\cdots,N,$ and

L_l, L_m : leakage & mutual inductances of coupled inductor

r : effective series resistance of the coupled inductor

s_k : switching function of active switch in kth phase

V_g, v_o : input and output voltages, respectively.

If s_k=1, the corresponding active switch S_k is turned on. If s_k=0, S_k is turned off. For the sake of

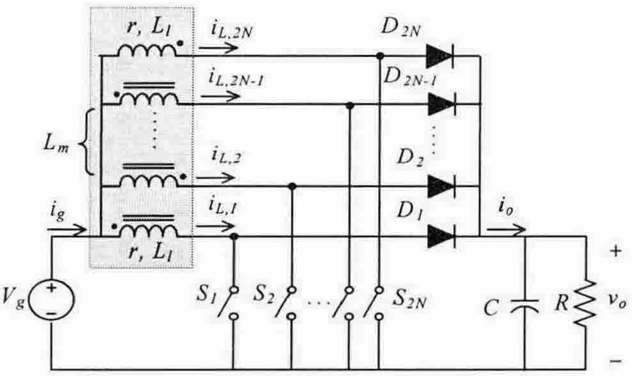

Fig. 1. 2N-phase IBC with coupled inductor

generality, the coupling parameter ρ has been introduced in (1). Depending on the winding orientation of the coupling inductor, ρ is defined as

$$\rho=\begin{cases}1 & \text{if } \textit{direct coupling}\\ -1 & \text{if } \textit{inverse coupling}\end{cases}$$

The generalized average state equation of the multi-phase IBC with coupled inductors can be expressed as

$$\dot{\bar{X}}=\bar{A}\bar{X}+\bar{B}u \tag{2}$$

The steady-state solutions for multi-phase IBC with coupled inductors are given in [2]. To derive the linearized small-signal model, the signals in the averaged state equation in (2) are perturbed about a quiescent dc operating point such as

$$\bar{x}=X+\tilde{x}(t)$$
$$\bar{d}=D+\tilde{d}(t) \tag{3}$$

where X and D are the quiescent values of the operating point, and $\tilde{x}$ and $\tilde{d}(t)$ denote small ac variations. The small-signal ac model for obtaining the transfer functions of interest can be found by expanding (2) in a Taylor series about the quiescent operating point and eliminating the dc and higher-order nonlinear terms.

There are 2N control inputs in the multi-phase IBC, which are the duty cycles. The duty cycles are controlled to be identical during a PWM period such as $d_k=d$, $k=1$, $\cdots$, $2N$. The small-signal ac model for the control-to-output transfer function can be obtained as

$$\dot{\tilde{X}}=\tilde{A}\tilde{X}+\tilde{B}\tilde{d} \tag{4}$$

where $\tilde{X}=[\tilde{i}_1\cdots\tilde{i}_{2N}\ \tilde{v}_0]^T$ and the matrices in (4) are given as

$$\tilde{A}=\frac{\partial f(\bar{X},U,D)}{\partial \bar{X}}\Big|_{\bar{X}=X},\quad \tilde{B}=\frac{\partial f(X,U,d)}{\partial d}\Big|_{d=D} \tag{5}$$

where $f(X,U,D)=\bar{A}X+\bar{B}U$. If (5) is written as

$$\tilde{A}=\begin{bmatrix}\tilde{A}_{11} & \tilde{A}_{12}\\ \tilde{A}_{21} & \tilde{A}_{22}\end{bmatrix},\quad \tilde{B}=\begin{bmatrix}\tilde{B}_1\\ \tilde{B}_2\end{bmatrix} \tag{6}$$

The following parameters can be found by evaluating (2) and using the relationship $N\beta+\gamma=1$, $\tilde{A}_{11}=A_1$, $\tilde{A}_{22}=A_2$

$$\tilde{A}_{12}=\left[0\cdots0\ -\frac{D'}{L_c}\right]^T\quad \tilde{A}_{21}=\left[0\cdots0\ \frac{2N}{C}D'\right]$$

$$\tilde{B}_1=\left[0\cdots0\ \frac{V_0}{L_c}\right]^T\quad \tilde{B}_2=\left[-\frac{2N}{C}I_{2N}\right]$$

The output equation can be expressed as

$$\tilde{y}=\tilde{E}\tilde{X} \tag{7}$$

where $\tilde{E}=[0\cdots0\ 1]$ and $\tilde{y}$ is the output or capacitor voltage. Therefore, the control-to output transfer function $G_{vd}(s)$ can be derived as

$$G_{vd}(s)=\frac{\tilde{v}_0(s)}{\tilde{d}(s)}\Big|_{\tilde{v}_g=0}=\tilde{E}(sI-\tilde{A})^{-1}\tilde{B} \tag{8}$$

Using Mathematica®, the control-to-output transfer function of the multi-phase IBC with coupled inductors can be found as

$$G_{vd}(s)=\frac{2NV}{(r+2ND'^2R)C}\frac{-s+(2ND'^2R-r)/L_c}{\left(s+\frac{r}{L_c}\right)\left(s+\frac{1}{RC}\right)+\frac{2ND'^2}{L_cC}} \tag{9}$$

The line-to-output transfer function $G_{vg}(s)$ and output impedance $Z_{out}(s)$ can also be derived as

$$G_{vg}(s)=\frac{\tilde{v}_0(s)}{\tilde{v}(s)}\Big|_{\tilde{d}=0}=\frac{2ND'/L_cC}{\left(s+\frac{r}{L_c}\right)\left(s+\frac{1}{RC}\right)+\frac{2ND'^2}{L_cC}} \tag{10}$$

$$Z_{out}(s)=\frac{\tilde{v}_0(s)}{\tilde{i}_0(s)}\Big|_{\tilde{d}=0}=\frac{1}{C}\frac{s+r/L_c}{\left(s+\frac{r}{L_c}\right)\left(s+\frac{1}{RC}\right)+\frac{2ND'^2}{L_cC}} \tag{11}$$

3. SIMULATED AND EXPERIMENTAL RESULTS

The generalized small-signal analysis in the previous sections is verified through the experimental results for single, two, and four-phase IBC. The parameters, used in the simulation and experiment, are as follows

$r\approx0.24\,\Omega$ (including the current-sensing resistance)

$C=22\,\mu F$, $ESR\ of\ C=0.3\,\Omega$, $R=21.6\,\Omega$, $V_g=7\ V$
$T_s=40\ \mu\text{sec}$

The self inductances of the coupled inductors are $L_k\approx600\,\mu H$. In order to verify the validity of the generalized transfer functions and output impedance, the theoretical results are compared with results obtained from PSpice frequency analysis. The duty cycle D is 0.67.

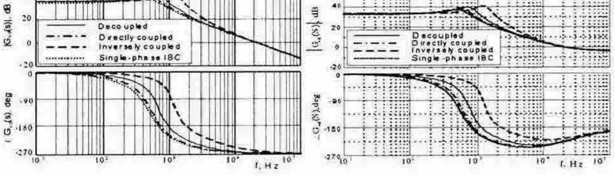

(a) 2-phase IBC

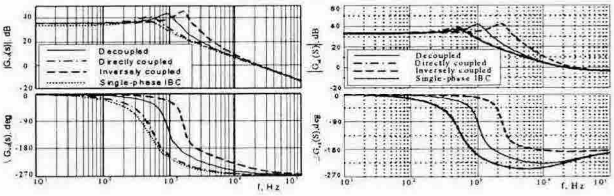

(b) 4-phase IBC

Fig. 2. Control-to-output transfer functions for various couplings (left: theoretical results, right:PSpice result)

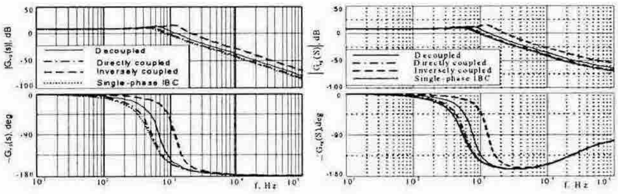

(a) 2-phase IBC

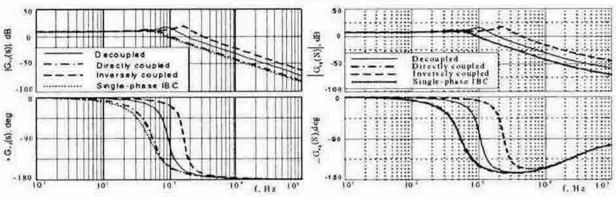

(b) 4-phase IBC

Fig. 3. Line-to-output transfer functions for various couplings (left: theoretical results, right:PSpice result)

Fig. 2 shows the control-to-output transfer functions according to the coupling methods. The theoretical bode plots are similar to the PSpice results except the high frequency range. Since the ESR of output capacitor is not zero in the PSpice simulation, the slope of magnitude rolloff decreases up to zero and the phase asymptote becomes -180°. Fig. 3 shows the line-to-output transfer functions according to the coupling methods. For the line disturbance, the line regulation is more deteriorated in case of the inversely or directly coupled inductor and when the IBC has more phases. Fig. 4 shows the start-up transient of the 4-phase IBC with different couplings. The IBCs with decoupled and inversely coupled inductors have faster dynamics and higher overshoots, which could be expected in the frequency analysis as shown in Fig. 2.

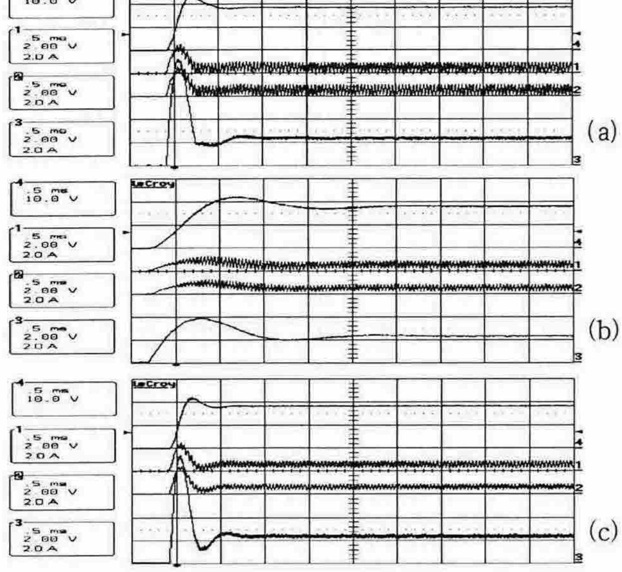

Fig. 4. Start-up transient of 4-phase IBC (upper: output voltage, middle: inductor currents, lower: input current): (a) decoupled, (b) direct, (c) inverse couplings

4. CONCLUSIONS

The multi-phase interleaved boost converter operated in the continuous inductor current mode has been analyzed according to the inductor couplings in small-signal. The analytical expressions for the generalized transfer functions of interest were derived from the transformed average state-space model and it was shown that the steady-state solutions are not dependent upon the inductor coupling. The theoretical results for the control-to-output, line-to-output transfer functions and the output impedance have been compared with the PSpice results.

This work was financially supported by MOCIE through IERC program.

REFERENCES

[1] P. Lee, Y. Lee, D. K. W. Cheng, and X. liu, "Steady-State Analysis of an Interleaved Boost Converter with Coupled Inductors", IEEE trans. on Industrial Electronics, Vol. 47, No. 4, pp. 787-795, August, 2000.

[2] H. B. Shin, J. G. Park, S. D. Chang, and H. Y. Choi, "Generalized analysis of multi-phase interleaved boost converter", Int Journal of Electronics, Vol. 92, No. 1, January, 2005.